

# High coupling piezoelectric thin films of Pb(Zr,Ti)O<sub>3</sub>-based ternary perovskite compounds for GHz-range film bulk acoustic resonators

N. Yamauchi,<sup>1,a)</sup> T. Shirai,<sup>1</sup> T. Yoshihara,<sup>1</sup> Y. Hayasaki,<sup>1</sup> T. Ueda,<sup>1</sup> T. Matsushima,<sup>1</sup> K. Wasa,<sup>2</sup> I. Kanno,<sup>2</sup> and H. Kotera<sup>2</sup>

<sup>1</sup>Advanced Technologies Development Laboratory, Panasonic Electric Works Co., Ltd., 1048, Kadoma, Osaka 581-8686, Japan

<sup>2</sup>Department of Micro Engineering, Kyoto University, Yoshida-honmachi, Sakyo-ku, Kyoto 606-8501, Japan

(Received 28 November 2008; accepted 8 April 2009; published online 28 April 2009)

We have deposited nearly stress-free single-crystal thin films of (001) Pb(Mn,Nb)O<sub>3</sub>-Pb(Zr,Ti)O<sub>3</sub> (PMnN-PZT) on (001)MgO substrates by rf-magnetron sputtering using a quenching process after the film growth. It is found that single *c*-domain/single-crystal thin films of PMnN-PZT containing 5%–10% PMnN show a strong hard ferroelectric response with  $2E_c \cong 400$  kV/cm and  $P_s \cong 70$   $\mu$ C/cm<sup>2</sup>. GHz-range film bulk acoustic resonators incorporating PMnN-PZT thin films have been fabricated with microelectromechanical system technology. The maximum electromechanical coupling coefficient  $k_t$  and mechanical quality factor  $Q_m$  were 0.7 and 185 in the 4 GHz range, respectively. © 2009 American Institute of Physics. [DOI: 10.1063/1.3126060]

Much attention has been paid to GHz thin film bulk acoustic devices including thin film bulk acoustic resonators (FBARs) for GHz mobile communication systems. At present piezoelectric thin films of AlN are considered the best materials for fabrication of FBARs, since thin film AlN exhibits high mechanical quality factor ( $Q_m$ ) greater than 1000, with moderately high coupling factor  $k_t^2$  ( $k_t^2 \cong 2\%$ – $6\%$  at GHz frequencies<sup>1</sup>). However, piezoelectric thin films with high  $Q_m$  values and higher coupling factors are essential for the fabrication of a variety of GHz thin film acoustic devices. It is expected that bulk Pb(Zr,Ti)O<sub>3</sub> (PZT) based ceramics [Pb(Mn,Nb)O<sub>3</sub>-doped PZT (PMnN-PZT)] show a variety of ferroelectric properties with high  $k_t^2$  ( $\cong 25\%$ ) and high  $Q_m$  ( $>1000$ ).<sup>2,3</sup> However, it is not clear whether the bulklike large  $k_t^2$  and  $Q_m$  will be reproduced in PZT-based piezoelectric thin films needed for GHz FBAR structures. The typical thickness of piezoelectric thin films is 200–300 nm and piezoelectric thin films exhibit microstructures with dislocated interfacial structures.<sup>4</sup> To achieve bulklike high coupling factors  $k_t^2$  with high  $Q_m$  values in the GHz range, thin films of single-crystal structure without dislocated interfaces are essential. Single-crystal films can be fabricated by heteroepitaxial growth using sputtering deposition. However, heteroepitaxial thin films contain dislocated interfacial structures and/or multidomain layers due to the growth stress.<sup>5</sup> Recently it was found that quenching after sputtering deposition resulted in heteroepitaxial thin films of single *c*-domain/single-crystal PMnN-PZT with smooth interfaces. These quenched thin films showed bulklike high transverse piezoelectric coefficients in the frequency range of 200–500 Hz.<sup>6</sup> This paper describes the microstructures and dielectric and piezoelectric properties of sputtered heteroepitaxial thin films of PMnN-PZT using the quenching process in relation to their applications for GHz thin film bulk acoustic devices.

Planar rf-magnetron sputtering was used for the heteroepitaxial growth of the PMnN-PZT thin films. The PMnN-PZT thin films were directly sputtered from a PMnN-

PZT powder target. The powder target was composed of a mixture of PbTiO<sub>3</sub>, PbO, Nb<sub>2</sub>O<sub>5</sub>, MnO<sub>2</sub>, ZrO<sub>2</sub>, and TiO<sub>2</sub>. The substrates were (001)Pt/(001)MgO with a buffer layer of (101)SrRuO<sub>3</sub> (SRO). The growth temperature and growth rate were  $\sim 600$  °C and  $\sim 200$  nm/hr. The sputtered thin films were quenched in air after the deposition. The cooling rates were 100 °C/min. Analysis using inductively coupled plasma emission spectrometry indicated that the chemical composition of the sputtered thin films was almost the same as the target composition.

Figure 1(a) shows a typical cross-sectional transmission electron microscopy (TEM) image of a sputtered PMnN-PZT thin film of 300 nm thickness. The cross-sectional TEM image suggests that the sputtered film has a high-density structure without grains or an interfacial layer near the substrate surface. Crystal structure analysis of the film after fast Fourier transform (FFT) indicates that the quenched sputtered films exhibit single *c*-domain/single-crystal structure, as shown in Fig. 1(b). The lattice image at the interface suggests the interface is coherent. Line defects were observed

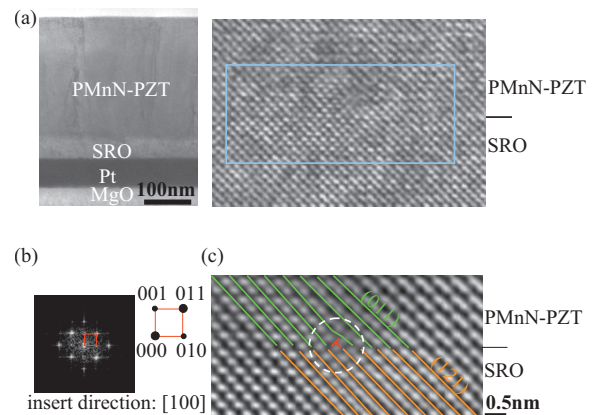


FIG. 1. (Color) (a) Cross sectional TEM image of sputtered 0.06PMnN-0.94PZT(48/52) thin film with 300 nm thickness, (b) corresponding FFT patterns of selected area of (a), and (c) high resolution TEM image after FFT from the original TEM image of (a).

<sup>a)</sup>Electronic mail: yamauchi.norihiro@panasonic-denko.co.jp.

TABLE I. Lattice parameters of sputtered PMnN-PZT thin films epitaxially grown on (101)SRO/(001)Pt/(001)MgO for different film thickness. Film composition: 0.06PMnN-0.94PZT(48/52). (101)SRO:  $a=0.393$  nm.

Thickness ( $\mu\text{m}$ )	Lattice parameters					
	$a$	$b$	$c$ (nm)	$\alpha$	$\beta$	$\gamma$ (deg)
Film 1.9	0.4043	0.4045	0.4148	90.0	89.9	90.0
0.3	0.398	0.4022	0.415	90.0	89.9	89.0
Bulk	0.4046	0.4046	0.4129	...	...	...

due to the lattice mismatch between PMnN-PZT thin films and SRO, as shown in Fig. 1(c).

Table I shows the typical lattice parameters of (001)PMnN-PZT thin films for different film thickness measured by in-plane x-ray diffraction analysis. The heteroepitaxial thin films are in the tetragonal phase as expected. The in-plane lattice parameters for the thicker film are almost the same as bulk values of PMnN-PZT and are independent of the substrate lattice parameters. This tendency is also observed in the Pb(Mg,Nb)O<sub>3</sub>-PZT (PMgN-PZT) thin films.<sup>7</sup> The sputtered films show reduced stress and/or a strain-relaxed structure. The in-plane lattice spacing for the thinner thin films (300 nm thickness) is slightly smaller than bulk value, indicating that in-plane compressive stress is present. However, the in-plane stress does not induce a dislocated interfacial layer as was seen in the cross-sectional TEM image. Antiphase-type planar defects are instead of a dislocated interface.<sup>8</sup>

Figure 2 shows a typical  $P$ - $E$  hysteresis curve for a single  $c$ -domain/single-crystal thin film of 0.06PMnN-0.94PZT(48/52). The hysteresis curve shows typical hard ferroelectric properties, i.e., square-shaped loops with high  $E_c$  and large  $P_s$  value ( $2E_c \cong 400$  kV/cm and  $P_s \cong 70$   $\mu\text{C}/\text{cm}^2$ ). The  $E_c$  value of the 300 nm film is two times larger than the  $E_c$  observed at the film thickness of 1.9  $\mu\text{m}$ .<sup>6</sup>

Piezoelectric coupling factors of the thickness vibration mode ( $k_t$ ) for the PMnN-PZT thin films were evaluated in the planar FBAR structure shown in Fig. 3. (001)MgO substrates 0.3 mm in thickness were used to fabricate the FBAR structure. The FBAR structure consisted of the PMnN-PZT thin film, SRO/Pt base conductive electrode and Al top electrode.

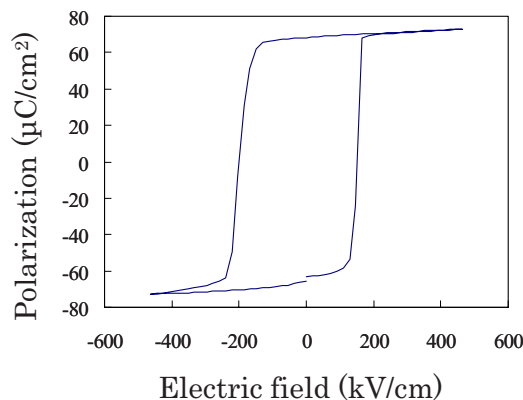


FIG. 2. (Color online) Typical  $P$ - $E$  hysteresis curve of (001)PMnN-PZT thin film epitaxially grown on (101)SRO/(001)Pt/(001)MgO substrate. PMnN-PZT film thickness: 300 nm, film composition: 0.06PMnN-0.94PZT (48/52).

The thickness of the PMnN-PZT, SRO/Pt, and Al electrodes were typically 280–320, 110, and 100 nm, respectively. The surface roughness of the PMnN-PZT thin films was 2–3 nm. The size of the Al top electrode was  $50 \times 50$   $\mu\text{m}^2$ . The back side of the MgO substrate was removed by chemical etching. The effective coupling factor  $k_{\text{eff}}$  was evaluated by the relation  $k_{\text{eff}} = [(f_p^2 - f_s^2)/f_p^2]^{1/2}$ , where  $f_p$  and  $f_s$  denote the parallel and series resonant frequency. The  $k_t$  was evaluated by the relation  $k_t^2 = (\pi^2/8)(k_{\text{eff}}^2)/(1 - k_{\text{eff}}^2)$ . The  $Q_m$  was obtained by the phase change in the impedance at antiresonant frequency using the relation  $Q_m = 1/2\omega(d\Phi/d\omega)$ . These resonant properties were evaluated by the Smith chart obtained by a network analyzer. A typical Smith chart and the phase change in the impedance for a PMnN-PZT thin film are shown in Fig. 4. From the analyses of the Smith chart it was found that thin films of 0.06PMnN-0.94PZT(48/52) of 300 nm film thickness showed  $f_s=3540$  MHz and  $f_p=4167$  MHz. Taking the observed  $f_p$  and  $f_s$  values, the  $k_{\text{eff}}$  and the  $k_t$  were 0.527 and 0.689, respectively. Thin films of intrinsic PZT(48/52) showed  $f_s=3724$  MHz and  $f_p=4451$  MHz. Their  $k_{\text{eff}}$  and  $k_t$  were 0.547 and 0.726, respectively.

The values of  $Q_m$  for PMnN-PZT and the PZT thin films were 157 and 114, respectively. These data suggest that doping of PMnN into PZT increases in  $Q_m$ . The coupling slightly decreases with the doping of PMnN similar to bulk ceramics.<sup>3</sup> In 0.1PMnN-0.9PZT(55/45) thin film,  $k_t$  and  $Q_m$  were 0.619 and 185, respectively.

The variations in the  $k_t$  and  $Q_m$  with the composition of PMnN-PZT thin films are shown in Fig. 5. In the figure the composition of the PZT is near the morphotropic phase boundary (MPB) composition. It is seen that the maximum  $k_t$  is realized in intrinsic PZT, while the  $Q_m$  increases with the addition of PMnN. The highest  $Q_m$  was obtained with the addition of PMnN of 5%–10% for the PZT near the MPB composition. The figure of merit  $k_t^2 Q$  for a design of wide-band filters for PMnN-PZT thin films was around 70. These values are much higher than previously reported PZT thin

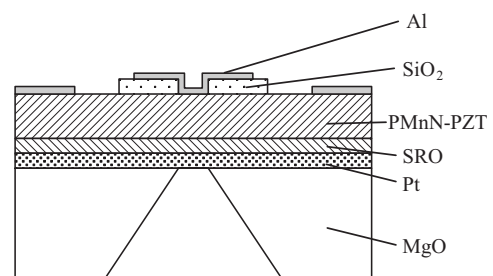


FIG. 3. Schematic drawing of PMnN-PZT FBAR structure.

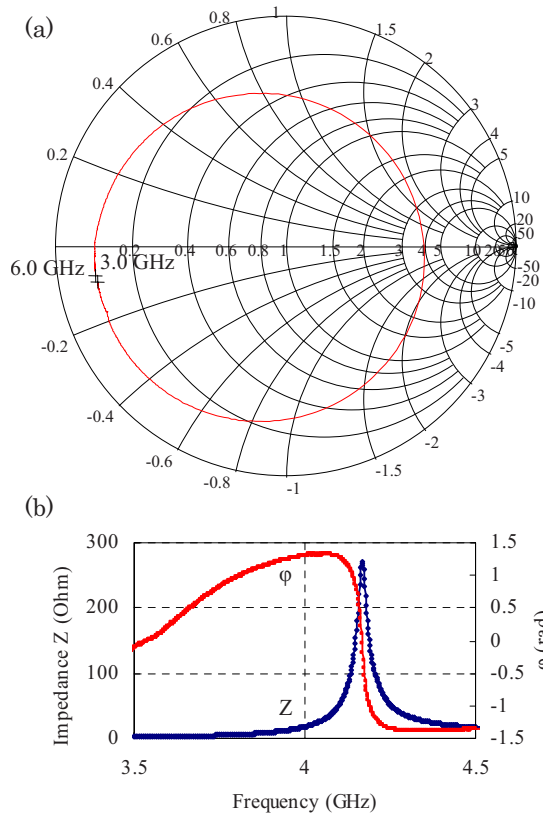


FIG. 4. (Color online) Typical Smith chart (a) and phase change in impedance (b) for a PMnN-PZT thin film: film composition 0.06PMnN-0.94PZT(48/52); film thickness, 300 nm.

film values,  $k_t^2 Q_m \sim 1-22$  (Ref. 1) and comparable to AlN FBAR,  $k_t^2 Q_m \sim 160$ .<sup>1</sup> From the equivalent circuit analysis for FBAR using the modified Butterworth–Van Dyke model,  $C_o$  was determined to be 6.5 pF with the relative dielectric constant of 88 for the PMnN-PZT thin film of 300 nm in film thickness in the GHz range. The dielectric constants of the thin films are one order of magnitude lower than the bulk

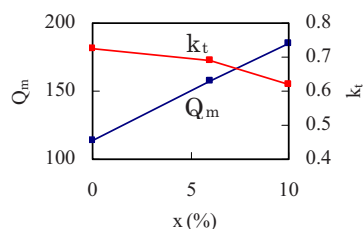


FIG. 5. (Color online)  $Q_m$  for different compositions of PMnN-PZT thin films. The coupling constants were much higher than the bulk ceramic values.

ceramics. Lower dielectric constants are essential for application in GHz devices.

The reason why the present PMnN-PZT thin films show higher  $Q_m$  than conventional PZT thin films are considered as follows: one reason is the microstructure of the present PMnN-PZT thin films. The present thin films show single-crystal-like high-density structures without interfacial layers. As shown in Fig. 1, the interface is coherent. The dislocated interfacial layer was absent, although line defects were present at the interface due to the lattice misfit of 3.6% between the lattice parameters, (121)SRO,  $d=2.78$  Å, and (011)PMnN-PZT,  $d=2.88$  Å. These line defects will not develop into dislocated layers and/or domain structures. The high  $k_t$  and high  $Q_m$  in the present sputtered intrinsic PZT films surely result from their structural perfection. A second reason is the relaxation effect of PMnN doping. Codoping with acceptor Mn and donor Nb enhances the hard ferroelectric properties similar to bulk ceramics. The highest  $k_t$  and  $Q_m$  values will be achieved with optimum doping of PMnN. In contrast, doping of PbTiO<sub>3</sub> with Pb(Mg,Nb)O<sub>3</sub> results in soft materials.<sup>9</sup> In conclusion, improvement of composition and microstructure of PZT thin films results in higher  $k_t$  and  $Q_m$  values. The present PZT-based ternary perovskite thin films can be applied in GHz FBAR and/or GHz planar ladder filters.

This study is a part of the Advancing Technology Excellence “Nano-Medicine” project, which is within the Kyoto City Collaboration of Regional entities assigned by Japan Science and Technology Agency. The authors thank Dr. T. Matsunaga of Panasonic Corporation for four-axis x-ray measurements.

<sup>1</sup>P. Muralt, J. Antifakos, M. Cantoni, R. Lane, and F. Martin, *Proceedings of the 2005 IEEE Ultrasonic Symposium* (IEEE, Rotterdam, 2005), Vol. 1, pp. 315–320.

<sup>2</sup>L. Eric Cross, in *Ferroelectric Ceramics*, edited by N. Setter and E. L. Colla (Birkhäuser, Basel, 1993), pp. 1–85.

<sup>3</sup>M. Takahashi, N. Tsubouchi, and T. Ohno, IEC Report No. CPM71-22, 1971 [in Japanese].

<sup>4</sup>J. D. Larson III, S. R. Gilbert, and B. Xu, *Proceedings of the IEEE Ultrasonic Symposium* (IEEE, Montreal, 2004), p. 173.

<sup>5</sup>B. S. Kwak, A. Erbil, J. D. Budai, M. F. Chisholm, L. A. Boatner, and B. J. Wilkens, *Phys. Rev. B* **49**, 14865 (1994).

<sup>6</sup>T. Zhang, K. Wasa, I. Kanno, and S.-Y. Zhang, *J. Vac. Sci. Technol. A* **26**, 985 (2008).

<sup>7</sup>K. Wasa, I. Kanno, and T. Suzuki, *Adv. Sci. Technol. (Faenza, Italy)* **45**, 1212 (2006).

<sup>8</sup>S. H. Seo, H. C. Kang, D. Y. Noh, Y. Yamada, and K. Wasa, *Appl. Phys. Lett.* **84**, 3133 (2004).

<sup>9</sup>K. Wasa, S. Ito, K. Nakamura, I. Kanno, T. Suzuki, H. Okino, T. Yamamoto, S. H. Seo, and D. Y. Noh, *Appl. Phys. Lett.* **88**, 122903 (2006).